The effect of ultrasound on crystallization-precipitation processes : some examples and a new segregation model

John A. Dodds, Fabienne Espitalier, Olivier Louisnard, Romain Grossier, René David, Myriam Hassoun, Fabien Baillon, Cendrine Gatumel, Nathalie Lyczko

The Effect of Ultrasound on Crystallisation-Precipitation Processes: Some Examples and a New Segregation Model

John Dodds, Fabienne Espitalier, Olivier Louisnard, Romain Grossier, René David, Myriam Hassoun, Fabien Baillon, Cendrine Gatumel, Nathalie Lyczko*

Abstract

This paper discusses the effects of ultrasound on the production of particles by precipitation and crystallization. Examples are given from the formation of crystals of $BaSO_4$, K_2SO_4, TiO_2 and sucrose. It is shown that ultrasound reduces the induction time, narrows the width of the metastable zone and leads to the production of more, finer, and more uniform crystals in some cases. The reasons for these effects of ultrasound on the nucleation of crystals are discussed and a possible mechanism is presented.

Keywords: crystallization, nucleation, precipitation, segregation model, ultrasound

1 Introduction

Ultrasound has been used for over 20 years to control the formation of solids in crystallization processes. Experiments have been reported where supersaturation has been generated by cooling (a solution or a melt), by addition of a solvent or by reaction. A large variety of products have been studied: inorganic (titanium dioxide, ammonium sulfate, aluminium alloy, zeolite...), organic (sugars, pharmaceutical drug or excipients, cocoa butter...) and ice. All this work shows that ultrasound has an effect on nucleation by shifting the size distribution towards small particles and modifying the morphology or the polymorphs synthetized. Ruecroft et al. (2005) presented two large scale industrial processes based on a flow cell with multiple transducers for a high insonation and a device using a combination of a vortex-mixing with a transducer for preparation of micron sized particles. However, the mechanism or the link between nucleation and ultrasonic cavitation remains unclear and uncertain (Ruecroft et al., 2005) and only a few papers have tried to quantify the observed phenomena. For example in a recent paper, Virone et al. (2005) attempted to correlate the collapse pressure of cavitation bubble with supersaturation and therefore with the nucleation rate. In their paper, they presented results for crystallization induction time determined in a system with a well-defined pressure profile avoiding uncontrolled reflection. It was shown that the induction times calculated from the nucleation as a function of local pressure and growth rate were much lower than those determined experimentally: 1 s instead of 30 min.

In the first part of this paper some characteristic results will be presented and in the second part, the modeling of molecular segregation by pressure gradients around a single cavitation bubble will be described. This is proposed as a mechanism for the effect of ultrasound on particle generation and some with practical consequences will be presented.

* J. Dodds, F. Espitalier, O. Louisnard, R. Grossier, R. David, M. Hassoun, F. Baillon, C. Gatumel, N. Lyczko, RAPSODEE, UMR-EMAC CNRS 2392, Ecole des Mines d'Albi-Carmaux, Campus Jarlard, 81013 Albi (France). E-mail: fabienne.espitalier@enstimac.fr; olivier.louisnard@enstimac.fr

2 Main Experimental Results

The main effects of ultrasound on the production of particles by precipitation and crystallization will be presented with examples from previous papers [3–5] involving $BaSO_4$, K_2SO_4, TiO_2 and sucrose (Gatumel et al. 1999, Lyczko et al. 2002, Baillon 2002, Hassoun et al. 2003).
In these experiments, the dissipated ultrasound power measured by calorimetry ranged from 0.01 to 0.15 W/g solution, except in the case of continuous precipitation of barium sulfate (1.6 W/g sol.). The frequency of ultrasound was 20–23 kHz. The results obtained from all these different studies, involving different products and using different ultrasonic transducers showed that ultrasound makes crystallization more reproducible. and that the major effect of ultrasound is on primary or of more reproducible and secondary nucleation.

Barium Sulfate

In the study of barium sulfate precipitation, two modes of precipitation were used: semibatch in a stirred vessel of 1.5 L and in continuous mode (Gatumel et al., 1999). The continuous mode was used to separate the nucleation step from the crystal growth step. The experimental equipment comprised two vessels in series: a tube cell (0.0501) and a stirred vessel (0.7851). Ultrasound was emitted respectively by a tip transducer in the small cell and from a large bottom surface in the 0.7851 vessel (Figure 1).

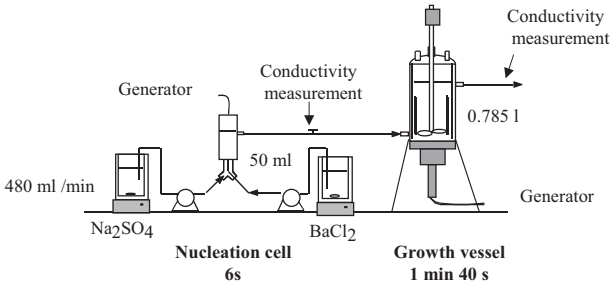

Fig. 1: Experimental equipment for continuous precipitation of barium sulfate (Gatumel et al., 1999).

Figure 2 shows the supersaturation ratio S at the outlet of the growth vessel as function of the supersaturation ratio at the outlet of the nucleation cell with or without ultrasound. The supersaturation ratio S is the ratio between the concentration and the equilibrium concentration. The concentrations are calculated from conductivity measurements. S was always lower at the outlet of the growth vessel than at the outlet of the nucleation cell

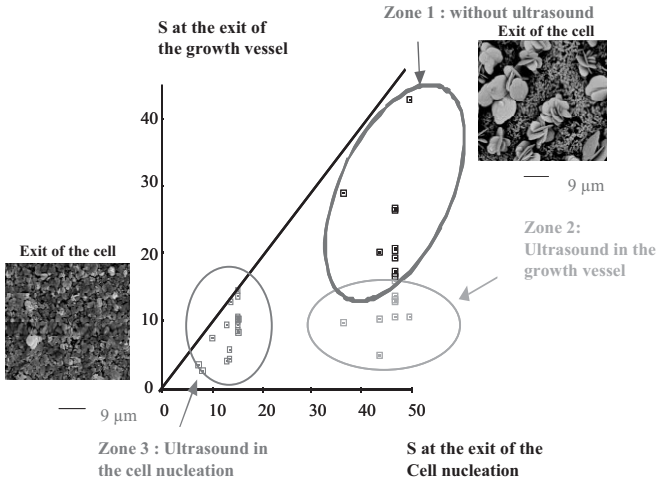

Fig. 2: Supersaturation ratio S at the exit of the growth vessel as function of the supersaturation ratio at the exit of the nucleation cell, with or without ultrasound (Gatumel et al., 1999).

due to the consumption of solute by growth or secondary nucleation in the growth vessel. Three zones can be identified: zone 1 corresponds to experiments with ultrasound, zone 2 to experiments with ultrasound in the growth vessel and zone 3 with ultrasound in the nucleation cell and eventually in the growth vessel. In all cases, the application of ultrasound brings about a decrease in S and in the mean surface diameter (Figure 3). In this figure, the numbers of crystals at the exit of two vessels

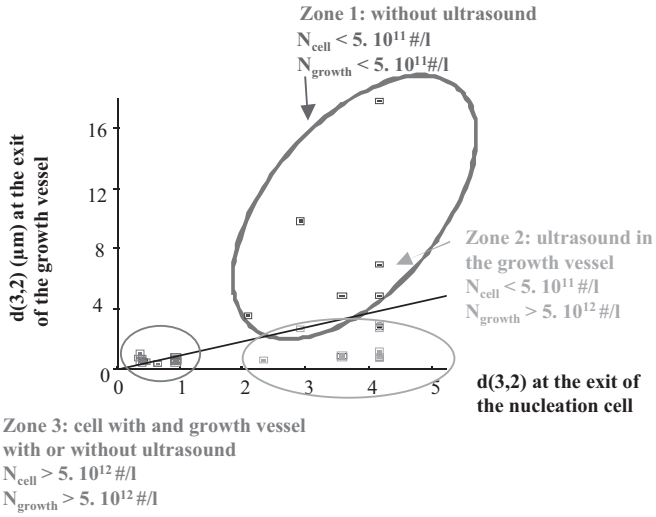

Fig. 3: Mean surface diameter at the exit of the growth vessel as function of mean surface diameter at the exit of the nucleation cell (Gatumel et al., 1999).

are given. In presence of ultrasound the number of crystals increases ten fold. This increase is directly linked with the decrease of the mean diameter. In addition on

Figure 2, shows the SEM pictures of crystals obtained at the exit of the cell with and without ultrasound. This indicates that for a dissipated power greater than 1.5 W/g sol, ultrasound modifies the morphology of crystals to make more uniform crystals than without ultrasound. Figure 4 presents the surface size distribution obtained at the exit of the nucleation cell (a) with and without ultrasound and at the exit of the growth vessel with or without ultrasound in the nucleation cell (b). The application of ultrasound narrows the particle size distribution and gives a monomodal distribution.

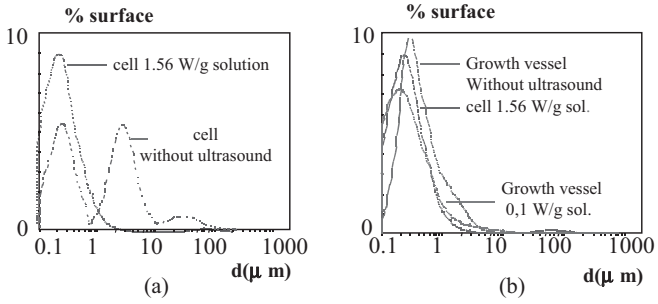

Fig. 4: Surface size distribution of $BaSO_4$ crystals at the exit of the nucleation cell (Gatumel et al., 1999).

Potassium Sulfate

Induction times have been measured at 15 °C in a vessel of 200 ml and 1 L for potassium sulfate (Lyczko et al., 2002). The experimental equipment (Figure 5) are thermostated vessels (0.2 L and 1L) respectively with a magnetic stirrer at a constant rotation speed of about 500 rpm and with a three-blade propeller (Mixel TT) at a constant rotation speed about 600 rpm. Ultrasound is respectively applied at the top of the vessel by a stainless ultrasound source with a titanium tip and at the base of the vessel with a cup-horn source (from Sinaptec Co.). Two ultrasonic powers levels have been measured: 0.05 and 0.12 W/g solution for the tip and 0.03 W/g solution for a cup horn source.

Saturated aqueous solutions were prepared from potassium sulfate crystals (synthesis grade 99,9%) and distilled water. The solution is rapidly cooled from the saturation temperature plus 5 °C to a final temperature of about 15 ± 0.4 °C. When this final temperature is reached, the conductivity solution is monitored in order to detect the appearance of the solid. The conductivity and the temperature of the solution were measured with an instrumental accuracy of about ± 0.1 mS/cm and ± 0.1 °C, respectively. Ultrasound is applied at the end of the cooling phase. In the 0.2 L vessel, the initial saturation temperatures ranged from 22 to 25 °C and from

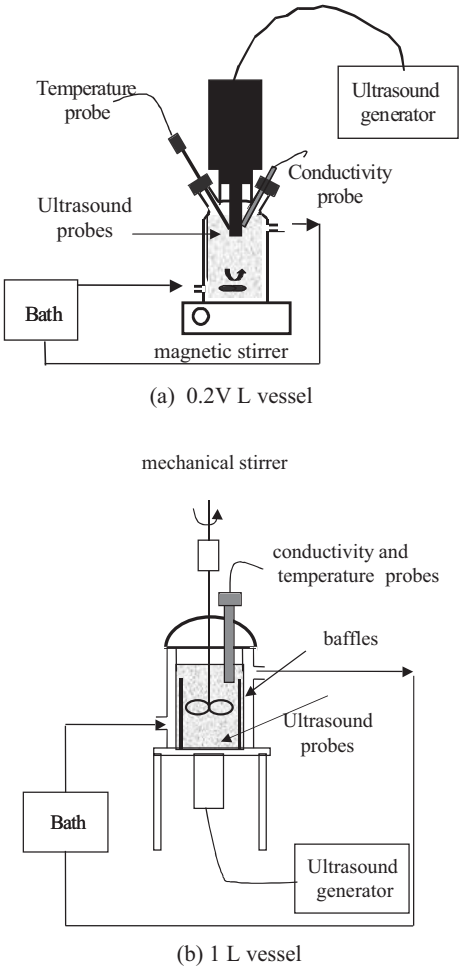

Fig. 5: Experimental equipments for potassium sulfate crystallization.

19.5 to 23 °C for experiments without and with ultrasound, respectively. In the 1 L vessel, the initial saturation temperatures ranged from 24 to 30 °C for experiments without ultrasound and from 19 to 25 °C for experiments with ultrasound.

Figure 6 presents the induction times at 15 °C for the two vessels as function of the absolute supersaturations, and it is seen that the induction time is greatly reduced in the presence of ultrasound (Lyczko et al., 2002). For instance, in the case of 0.2 L vessel, for absolute supersaturations higher than 0.018 g de solid/g water, ultrasound has no influence on the induction time. For absolute supersaturations lower than 0.012 g de solid/g water, the induction time decreases as the ultrasonic power increases: the effect of ultrasound seems to be greater at low absolute supersaturation.

The experimental procedure for crystal recovery is summarized on Figure 7. For experiments carried out in the first apparatus, the magnetic stirrer is replaced by a mechanical stirrer when the crystals start to appear. This

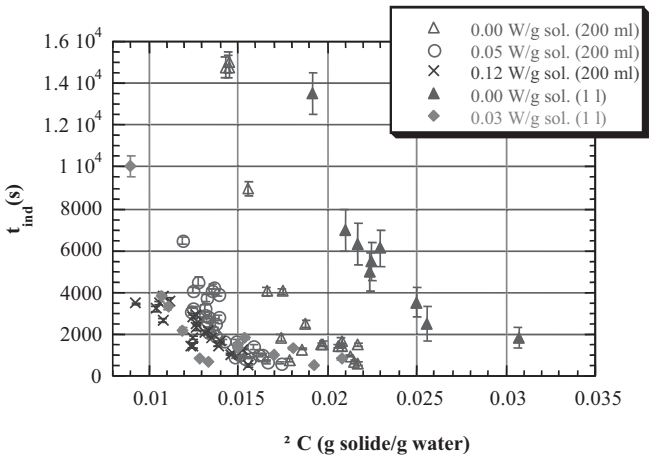

Fig. 6: Induction time as function of absolute supersaturation for potassium sulfate at 15 °C assuming an activity coefficient ratio close to 1 (Lyczko et al., 2002).

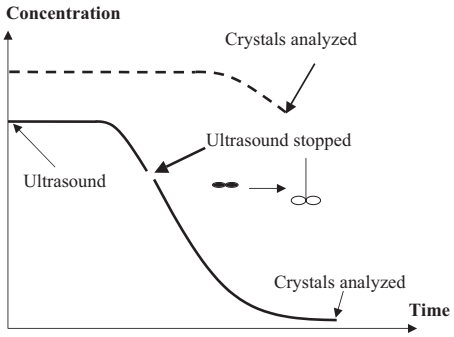

(a) 0.2L vessel

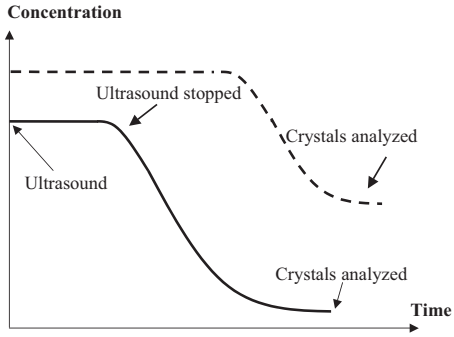

(b) 1L vessel

Fig. 7: Experimental procedure, – – – without ultrasound, — with ultrasound.

change is necessary to maintain the potassium sulfate crystals in suspension in the solution. For experiments without ultrasound, crystals are left growing for only 10 minutes, as they become too large to be analyzed after that duration. For experiments with ultrasound, the ultrasound is stopped after the nucleation step and crystals are left growing for one hour. For all experiments in the second apparatus, crystals grow for one hour from the moment they are detected,. The suspension is then filtered with a 0.45 µm pore diameter filter and the crystals are dried in an oven at 100 °C during 24 hours. The crystals numbers have been measured by a particle counter (Coulter Multisizer II).

Figure 8 shows, the number of crystals per unit volume against the absolute supersaturation for experiments with and without ultrasound, in the two experimental apparatus. In each vessel more crystals are formed in

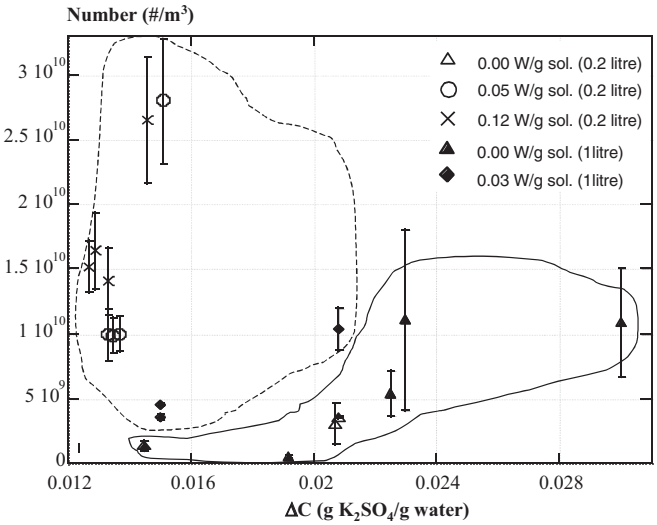

Fig. 8: Number of crystals formed, – without ultrasound; – – – with ultrasound.

presence of ultrasound. For an equivalent absolute supersaturation (0.015 g K_2SO_4/g water), the number of crystals is about 3.10^8 #/m^3 without ultrasound and higher than 2.5 10^{10} #/m^3 with ultrasound. Thus, ultrasound enhances the production of crystals. For experiments without ultrasound, more crystals are formed in the 0.2 L vessel than in the 1 L vessel and the same observation can be made for experiments with ultrasound. Therefore, the tip transducer seems more efficient that the "cup-horn".

For the two following studies (titanium dioxide and sucrose crystallization), the ultrasonic power reported throughout the paper is the active power indicated by the sonotrode generator and therefore is only an indication of the power really transmitted to the solution.

Titanium Dioxide

In the case of titanium dioxide, the induction time is about 30–35 min without ultrasound, is less than 25 min

for a power of 60 W and less than 10 min for a power of 100 W at 100 °C (Baillon, 2002). For this product, the morphology is unchanged (Figure 9). In order to identify the crystals obtained, the X-ray diffraction patterns for titanium dioxide powders collected at the end of precipi-

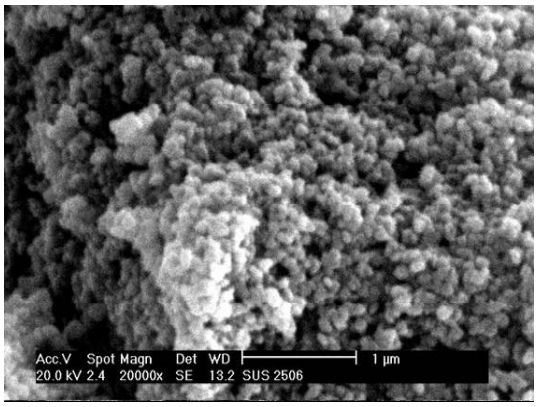

(a) without ultrasound

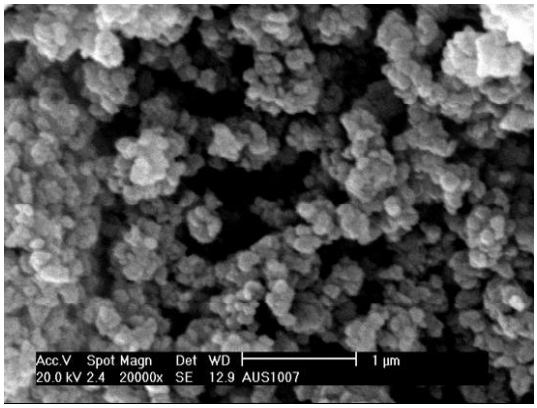

(b) with ultrasound 100 W

Fig. 9: SEM photographs of titanium dioxide crystals at moderate supersaturation without and with ultrasound.

tation have been acquired in a range of 2 µ from 20° to 75° by steps of 0.020°. For every point, the intensity data have been collected over 5 s. Figure 10 and Figure 11 show patterns obtained for powders produced by the hydrolysis of moderately and highly supersaturated solutions (respectively around 3000 and 8000), with and without ultrasound. The patterns have been deliberately shifted vertically for easier reading. Without ultrasound, it is seen that the pattern is characteristic of a pure anatase TiO_2 powder. On the other hand, with ultrasound, the XRD pattern also reveals the presence of a certain quantity of rutile within a matrix of anatase at low and high supersaturation. In order to clarify the influence of supersaturation, Figure 12 shows the refined XRD patterns (fine acquisition on the restricted 2 µ range between 20° and 32° by steps of 0.005°) for two experiments with ultrasound, respectively at low and high supersaturation. It appears that in the former case, the product is mainly anatase, as shown previously, while in the latter, the pattern is clearly biased toward the rutile reference peak. Thus, for strong supersaturation, the application of ultrasound orients markedly the precipitation towards the rutile form. Deconvolution of the peak leads to an estimation of 60 % for the mass-fraction of rutile in the final powder.

Sucrose

Sucrose crystallization has been studied in batch and continuous mode (Hassoun, 2003, Hassoun et al. 2003). Only results concerning continuous mode are reported in this paper. The crystallization was performed at 40 °C with a feed concentration of 76 % (w/w) and a feed flowrate of 0.15 l/min. Under these operating conditions, no crystals appeared in the 1.5 L crystallizer and in this particular case, ultrasound can be used to induce nucleation by a brief insonation or applied continuously in order to maintain a low size. The latter mode was chosen.

The size distributions obtained in the steady state have been measured by acoustic attenuation (Ultrasizer, MALVERN) for different ultrasound powers. The operating conditions are given in Table 1. On Figure 13, the mean volume diameter d[4,3] and the variation of concentration between the entrance and the exit of the crystallizer $\Delta C_{E\text{-}S}$ are reported. The d[4,3] decreases for a ultrasonic power between 25 and 35 W and stays constant for ultrasonic power higher than 35 W. $\Delta C_{E\text{-}S}$ is highest at 25 W and therefore the absolute supersaturation is lower. At this power ultrasound would have only not act on nucleation, but growth will also be favored: crystals would therefore be bigger. For ultrasound powers higher than 25 W, the phenomenon of cavitation seems to increase with ultrasound power, leading to more nucleation, and as a result the creation of a bigger number of small crystals. For ultrasound power higher than 30 W, the size of the particles does not vary any more. This phenomenon was already noted during the study of the crystallization of barium sulfate under ultrasound. It can be explained by a phenomenon of autodamping of ultrasound with high ultrasonic power. When the ultrasonic power increases, the number of cavitation bubbles becomes more important and holds up the spread of the wave which then becomes less efficient.

The semi-logarithmic plot of the population density according to the size of crystals for different ultrasound power (25–70 W) reveals some deviations from predictions from the model for a MSMPR type crystallizer (Mixed Suspension Mixed Product Removal) (Fig-

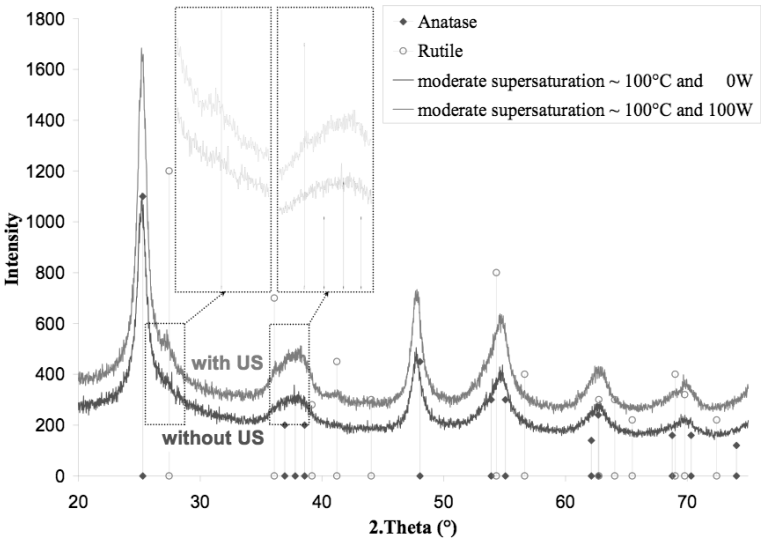

Fig. 10: XRD patterns obtained from thermal hydrolysis for titanium dioxide at moderate supersaturation with and without ultrasound.

ure 14). This phenomenon was already be noticed in the case of sucrose crystallizations (Hartel, 1980 and 1993) and were attributed to a growth rate dependent on the size of crystals. The growth rate, G, has been described by the model of Abbeg, Stevens and Larson:

$$G(L) = G_0\left[1+\frac{L}{G_0\tau}\right]^b$$

where G_0 is the growth rate of small crystals and b describes the effect of size on the growth rate. With this type of law for the growth rate, the population balance for a MSMPR crystallizer can be rewritten:

$$n(L) = n_0\left[1+\frac{L}{G_0\tau}\right]^{-b}\exp\left[\frac{1-\left[1+\left(L/G_0\tau\right)^{(1-b)}\right]}{1-b}\right].$$

The values of n_0 (the population density for the zero size), G_0 and b have been identified (Table 2).
The experiment at 25 W is not taken in to account. The growth rates are all of the same order $6.42 \pm 0.5\ 10^{-10}$ m/s. This therefore implies that for an ultrasound power higher than 30 W the growth rate does not increase any more. We can note a slight difference on the growth rate calculated at 50 W. The calculated growth rate of 10 µm crystals is comparable with those obtained by other authors without ultrasound in the same range of supersaturation (Hartel, 1980, Hartel 1993). The population densities obtained with ultrasound are 100 to 1000 times higher than those reported in the literature with higher residence time.
The density at zero n_0 increases according to applied ultrasound power. Therefore in most cases ultrasound would have an influence on nucleation rate: the higher the applied power the greater the number of created germs created.
For two experiments at 25 and 70 W, ultrasound was stopped after the steady state regime has been attained. The sucrose concentration was followed for one hour after this interruption (Figure 15 for P = 25 W): the sucrose concentration is constant. It seems that ultrasound initiates the crystallization, after this initiation ultrasound can be stopped or applied alternatively.
In all the three cases (K_2SO_4 crystallization by cooling, or $BaSO_4$ reactive crystallization), ultrasound brings about an increase in the number of crystals and a decrease in their size. All this at equivalent supersaturation and without modifying the crystalline structure if the solid does not present polymorphs. Other experiments with TiO_2, not reported here also confirm these conclusions. In addition it was found that the use of ultrasound induced a change in crystalline structure if the solid presents polymorphs. Moreover, despite the sucrose solution viscosity being a 100 to 3000 times higher than the viscosity of water at the same temperature, the effects of ultrasound are found to be identical as previously mentioned: decrease of induction time and increase of the nucleation rate.
Different explanations for these effects caused by ultrasound have been proposed in the literature: – the direct effect of high pressure arising around cavitation bubbles, or the effect of rapid local cooling rates-, however, none

Table 1: Operating conditions for Sucrose crystallisation.

Puissance (W)	C_E (%)	C_S (%)	C_E–C_S (%)	ΔC en sortie (%)
70	75.72	74.41 ± 0.20	1.31	3.91
50	75.80	74.49 ± 0.17	1.31	3.99
35	75.72	74.71 ± 0.19	0.98	4.24
30	75.72	74.49 ± 0.18	1.23	3.99
25	76.25	74.30 ± 0.21	1.96	3.8

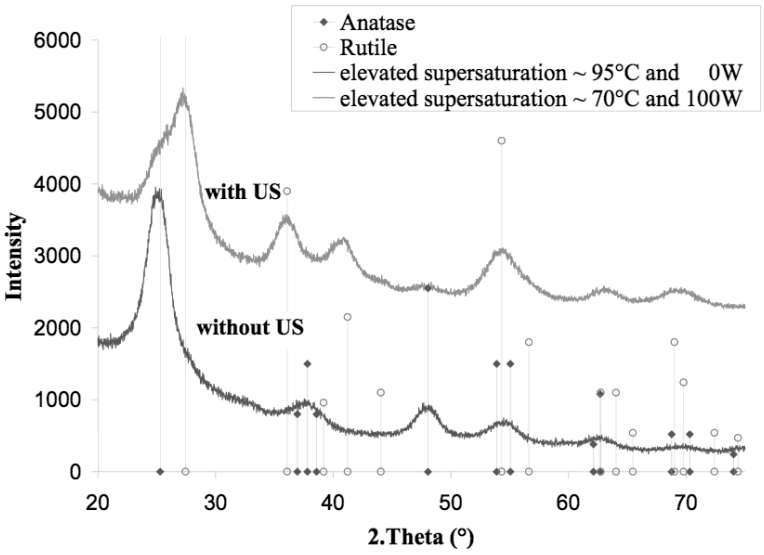

Fig. 11: XRD patterns obtained from thermal hydrolysis at high supersaturation with and without ultrasound in the case of titanium dioxide.

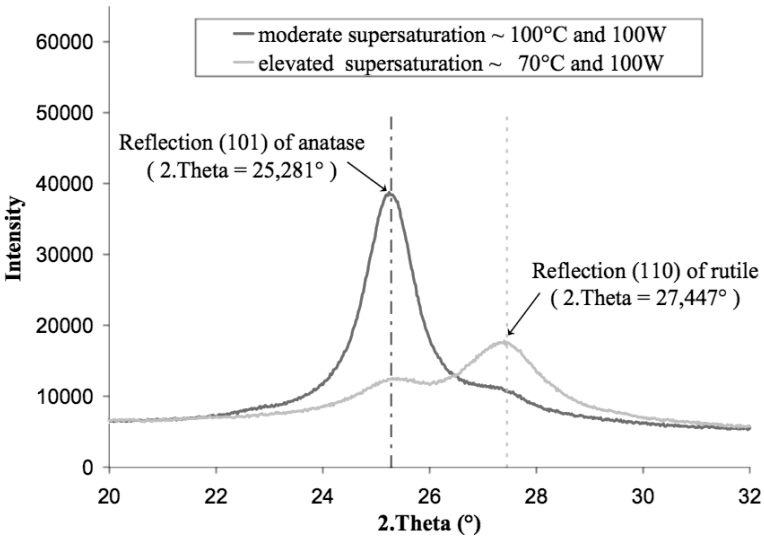

Fig. 12: XRD patterns obtained from thermal hydrolysis at moderate and high supersaturation with ultrasound in the case of titanium dioxide.

of them has been demonstrated clearly either by modeling or by experiments (Ruecroft et al., 2005). In the following we present an alternative hypothesis based on the molecular segregation of a liquid mixture by cavitation bubbles.

3 Segregation Model

The apparent effects of ultrasonic cavitation on nucleation are the same that one would obtain by increasing supersaturation: more numerous and small crystals, nucleating more rapidly. A naive question would therefore be: could cavitation increase supersaturation? In classical cavitation experiments, the liquid composition is homogeneous and in mechanical equilibrium, so that supersaturation can be defined at the macroscopic scale. In the case of a liquid undergoing acoustic cavitation, microscopic bubbles are driven in radial oscillation by the sound field. For a sufficiently high excitation, the bubble motion is mainly driven by the inertia of the liquid: after a large expansion phase during the field depression phase, the bubble collapses very quickly on a time-scale of the order of several ns. This phenomenon is repeated at each acoustic period, for billions of bubbles. Under these conditions, it is easily conceivable that there is no mechanical equilibrium at the microscopic scale in the liquid, possibly resulting in local variations of supersaturation, but the precise phenomenon involved remains to be identified.

Pressure gradients may be a possible source of mixture segregation. Following diffusion theory (Hirschfelder et al., 1967; Bird et al., 1960), when a mixture of two species is submitted to a pressure gradient, the lightest of the two is pushed toward low pressure regions. This forced diffusion process, known as pressure diffusion, remains generally weak but is commonly invoked to explain slow sedimentation in a still fluid mixture, or in ultracentrifuge applications where it is used profitably to separate species of large molecular weight from a solvent (Archibald, 1938). Since the outward acceleration of the bubble at the end of its collapse is about twelve orders of magnitude higher than gravity, it is conceivable that the corresponding huge pressure gradient would segregate very efficiently the species present in the liquid.

To explore this issue, we have developed a perturbation method to solve the convection-diffusion mass transport equation of a species in a binary mixture around a single cavitation bubble, including the pressure diffusion effect (Louisnard & al., 2006). The transport equation reads

$$\frac{\partial C_A}{\partial t} + v.\nabla C_A = D\nabla.(\nabla C_A + \tilde{\beta} C_A \nabla p) \qquad (1)$$

where C_A is the mass-fraction of species A, v(r,t) and p(r,t) are respectively the radial velocity and pressure field around the oscillating bubble, and D is the diffusion coefficient of species A in the mixture. The para-

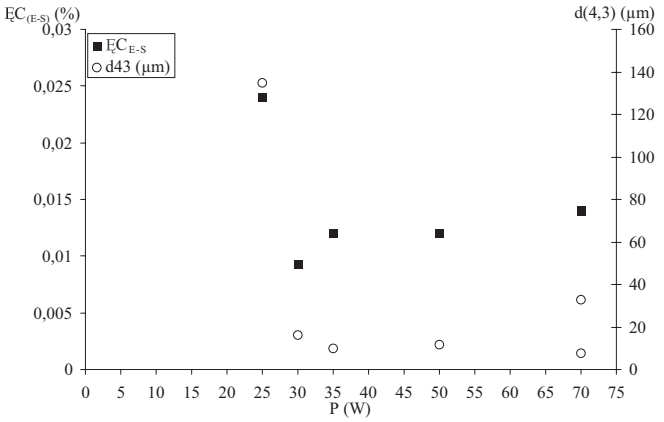

Fig. 13: d[4,3] at the exit of the sucrose crystallizer and $\Delta C_{E\text{-}S} = C_e - C_s$ as function of the ultrasound power.

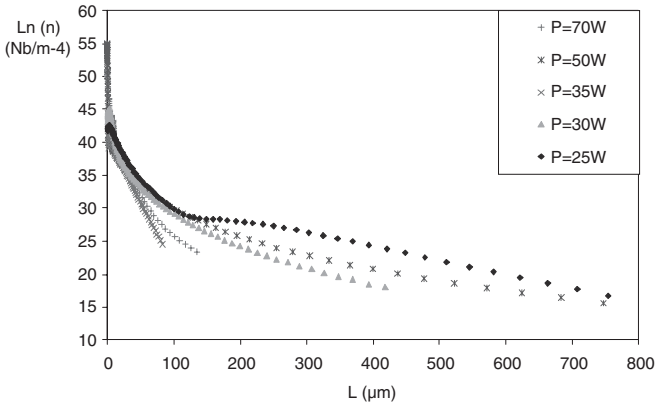

Fig. 14: Semi-logarithmic plot of the population density according to the size of crystals for different ultrasound power.

meter $\tilde{\beta}$ is the segregation parameter linked to the difference between the apparent densities of the two species:

$$\tilde{\beta} = \frac{M_A}{RT}\left(\frac{\overline{V}_A}{M_A} - \frac{\overline{V}_B}{M_B}\right). \qquad (2)$$

Table 2: Calculated values of G0, n0 and b for different ultrasound power in the case of Sucrose

$$G(L) = G_0\left[1 + \frac{L}{G_0\tau}\right]^b$$

Ultrsasound power (W)	τ(s)	G_0(m/s)	n_0(nb/m^{-4})	b	J (nbre/m^3/s)
30	502	$9.6*10^{-10}$	$4.9*10^{20}$	0.67	$4.7\ 10^{11}$
35	509	$7.6*10^{-10}$	$22.7*10^{20}$	0.59	$17.3\ 10^{11}$
50	570	$1.3*10^{-10}$	$39.0*10^{20}$	0.81	$5.1\ 10^{11}$
70	502	$7.2\ 10^{-10}$	$80.0\ 10^{20}$	0.59	$57.6\ 10^{11}$

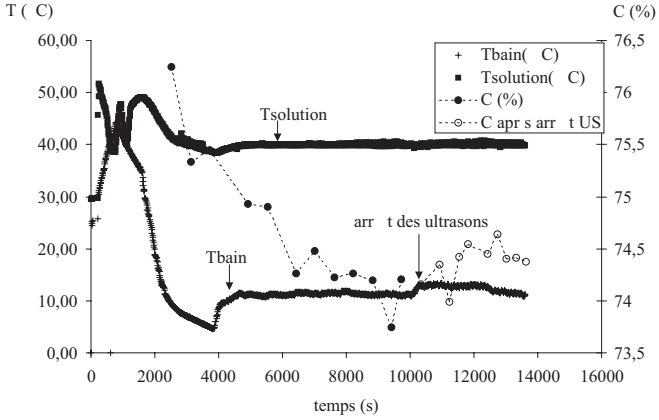

Fig. 15: Concentration and temperature as function of time at 25 W in the case of the Sucrose crystallization.

where M_i and $\overline{V}_i$ are the molecular weight and partial molal volume of species i, respectively. It must be noted that the theory remains valid if one of the species, say A, is replaced by sufficiently small particles (typically at the nanoscopic scale):in this case $\overline{V}_A/M_A$ represents $1/\rho_A$ the inverse of the density of the particle material and the molecular weigth is calculated by $M_A = N_{av}\rho_A V_A$, where N_{av} and V_A is respectively the Avogado's number and the particle volume. The approximate analytical solution obtained yields the concentration of species A at the bubble wall in the following form:

$$\frac{C_A(t,0)}{C_{A0}} = \exp(\beta I)\left[1 - \beta\left(\frac{D}{\omega R_0^2}\right)^{1/2} G(t)\right] \qquad (3)$$

where C_{A0} is the mass-fraction of A in the undisturbed mixture, I is a positive constant, $G(t)$ an oscillating function, and β is the dimensionless version of the segregation parameter $\tilde{\beta}$. Both quantities I and $G(t)$ depend on the bubble dynamics and can be easily calculated once the time-dependant bubble radius is known. In the case of inertial cavitation, where the bubbles collapse violently at each acoustic period, $G(t)$ is mainly a large positive short pulse repeating periodically at the end of the bubble collapse, lingering on a time-scale of several ns.

In order to obtain a global picture of the segregation phenomenon, it is interesting to calculate the quantities:

$$\Omega_m = \exp(\beta I) \qquad (4)$$

$$\Delta\Omega_m = -\beta \exp(\beta I)\left(\frac{D}{\omega R_0^2}\right)^{1/2} G_{max} \quad (5)$$

for a given mixture around a typical cavitation bubble driven at increasing power levels. The quantity Ω_m is the segregation rate at the bubble wall averaged over one bubble cycle and $\Delta\Omega_m$ is the peak value of the variation of the segregation rate, reached at the end of each bubble collapse. When $\beta = 0$, pressure diffusion does not act and we recover an unsegregated mixture. When $\beta < 0$ (A is in this case the heaviest species), Ω_m is lower than 1, which means that on average species A is depleted at the bubble wall, and $\Delta\Omega_m$ is positive, so that the mixture is overconcentrated periodically at each bubble collapse.

As an example, we consider a mixture of water with spherical copper nanoparticles, with radii ranging from 1 nm to 10 nm. The diffusion coefficient D is calculated from Stokes-Einstein theory. The bubble is assumed to be filled of air, has a radius of 4 μm at rest, and is driven by an acoustic field of frequency 20 kHz, which amplitude ranges from 0.8 to 1.6 bar, which are typical values in cavitation experiments.

The results are displayed in Figure 16: the absissa of both graphs is the amplitude of the acoustic field driving the bubble. Figure 16 (a) represents the average depletion Ω_m of particles at the bubble wall, while Figure 16 (b) represents the amplitude $\Delta\Omega_m$ of the periodic particles over-concentration. It can be seen on the left graph that the particles progressively disappear from the bubble wall, as either the amplitude or the particle size is increased. On the right graph, it can be seen that as the particle size is increased at fixed P, the over-concentration $\Delta\Omega_m$ first increases, and then decreases again for very large molecules. Similarly, for fixed particle size, $\Delta\Omega_m$ crosses a maximum as P increases (visible on the 5 nm and 10 nm curves). Combining the results of the two graphs, the following qualitative conclusions can be drawn:

- for small particles or low forcing amplitude, $\Omega_m \approx 1$, $\Delta\Omega_m \approx 0$: the mixture remains almost unsegregated (see filled circles symbols on Figure 16),
- for medium particles or medium forcing amplitude, $\Omega_m < 1$, $\Delta\Omega_m$ large: particles are slightly depleted at the bubble wall, but largely over-concentrated at each bubble collapse (see filled squares symbols on Figure 16). Note that this overconcentration may reach more than 2 orders of magnitude,
- for large particles or large forcing amplitude, $\Omega_m \approx 0$, $\Delta\Omega_m \approx 0$: particles are almost completely depleted at the bubble wall, and the over-concentration is small again (see open circles symbols on Figure 16), so that the particles are constantly held far from the bubble in this case.

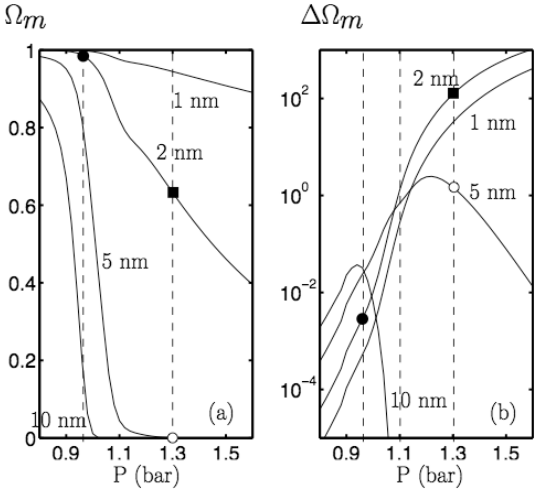

Fig. 16: Average (a) and periodic (b) concentration fields in a mixture of water with copper nanoparticles around a 4 μm air bubble driven by a 26.5 kHz acoustic field of various amplitudes P.

We now turn to apply these results to homogenous nucleation of crystals. Following classical nucleation theory (Kaschiev 2002), the lowest energy expense for a first-order phase transition is achieved by the progressive aggregation of solute molecules to form molecular clusters. These clusters have the density of the new phase and they must reach a critical size, referred as ''nucleus'' for the transition to occur. Therefore, the nucleation time is mainly the time required for the clusters to reach this critical size, and any microscopic effect enhancing the formation of the smallest clusters may reduce the nucleation time.

Clusters may grow by aggregation of solute molecules one by one with existing smaller clusters, as schematically displayed in Figure 17, where we have labeled the solute molecules by C_1 and a cluster formed by n molecules by C_n. Direct aggregation between two clusters C_m and C_n is generally neglected since they are much less numerous in solution than solute molecules. It should be noted that clusters do have physical reality and they have been evidenced for example by Mullin and Leci (1969) by gravity-driven sedimentation. This is in fact a pressure diffusion effect, due to the densities difference between the solution and the clusters.

Therefore, on the basis of above-described results on segregation, it is expected that clusters could be efficiently segregated by a cavitation bubble, in the following way:

- Solute molecules and small clusters would be remain unsegregated,
- Medium clusters would be periodically over-concentrated near the bubble wall at each bubble collapse (up to 2 orders of magnitude). This would favour not

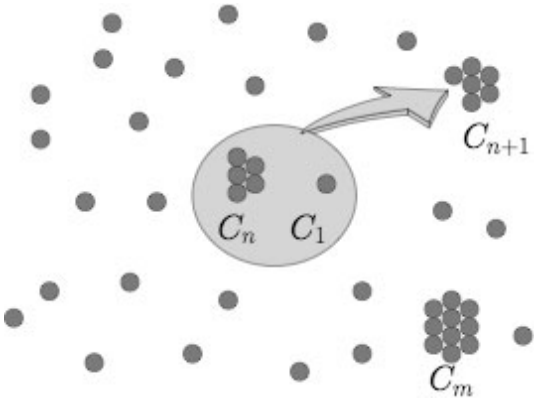

Fig. 17: Cluster growth by aggregation of a solute molecule C_1 on an existing cluster C_n, following classical nucleation theory. Direct aggregation between clusters C_m and C_n has low probability to occur because of the low number of clusters compared to solute molecules.

only their attachment to solute molecules, but would also enhance the generally neglected direct aggregation between two clusters (Figure 18), thus considerably increasing the overall nucleation rate.

- Large clusters would be finally pushed far from the bubble by the average effect. Again, this favours nucleation kinetics, in virtue of Le Chatelier principle since the ultimate products of the aggregation reactions will be constantly removed from the bubble wall.

In conclusion, a cavitation bubble, by the drastic segregation effect it produces in the surrounding liquid, would promote nucleation by acting as a cluster attachment reactor. Other possible microscopic mechanisms remain to be explored (direct dependance of supersaturation on pressure, solvent evaporation in the bubble),

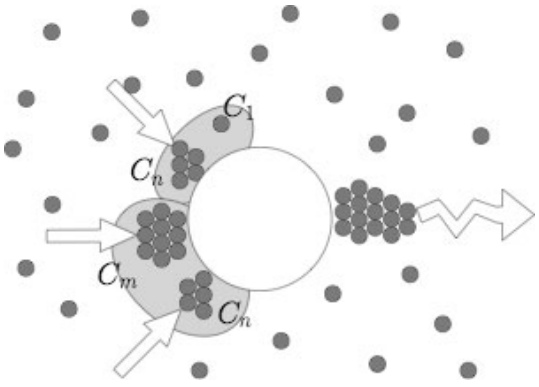

Fig. 18: Cluster growth in presence of a cavitation bubble: pressure diffusion concentrates medium clusters near the wall of the bubble at each collapse, favouring aggregation between these clusters and a solute molecule, and possibly giving direct aggregation between two clusters. Large clusters are then held far from the bubble by the average effect.

but our calculations show that segregation is a potential candidate for the macroscopically-observed nucleation enhancement. Furthermore, an experimental study based on microscopic planar laser induced-fluorescence is in progress to assess the physical reality of the segregation phenomenon around a single bubble (Grossier et al., 2006).

4 Conclusions

Results are presented for several series of experiments on the formation of crystals of $BaSO_4$, K_2SO_4, TiO_2 and Sucrose, both with and without application of ultrasound. These experiments show, as have those of others, that ultrasound has an effect on nucleation resulting in finer more uniform crystals. There is as yet no well established explanation of how these effects are caused. Here we present a new hypothesis based on the segregation in a liquid mixture by pressure gradients induced by cavitation bubbles. This theory seems to be in qualitative agreement with the phenomena found in crystallisation with ultrasound and an experimental programme based on the observation single cavitation bubbles is at present underway to make a quantitative test of the hypothesis.

5 References

[1] W. J. Archibald, The process of diffusion in a centrifugal field of force, *Phys. Rev.*, *53*, 746–752, **1938**.

[2] F. Baillon, Procédé de synthèse du dioxyde de titane: analyse et modélisation des solutions Titane-Sulfate; influence des ultrasons sur la précipitation, Doctorat de l'Ecole des Mines de Paris, spécialité Génie des Procédés, 24 Janvier **2002**.

[3] R. B. Bird, W. E. Stewart, E. N. Lightfoot, Transport phenomena. John Wiley and Sons, **1960**.

[4] C. Gatumel, F. Espitalier, J. Schwartzentruber, B. Biscans, A. M. Wilhelm, Nucleation control in precipitation processes by ultrasound, KONA *Powder and Particle* **1999**, *16*, p. 160–169.

[5] R. Grossier, O. Louisnard, Y. Vargas, Mixture segregation by an inertial cavitation bubble, submitted to *Ultrasonics Sonochemistry*, **2006**.

[6] J. O. Hirschfelder, C. F. Curtiss, R. B. Bird, Molecular theory of gases and liquids, John Wiley and Sons, **1967**.

[7] R. W. Hartel, A kinetic study of the nucleation and growth of sucrose crystals in a continuous cooling, crystallizer, PhD study –Doctor of Philosophy: Colorado, Fort Collins **1980**, pp. 1140.

[8] R. W. Hartel, Crystallization kinetics for the sucrose-water system, AICHE symposium Series, design, control and Analysis of crystallisation processes, **1993**, *76*, pp. 65–72.

[9] M. Hassoun, Criblage des paramètres influant sur la cristallisation par refroidissement d'un produit organique assistée par ultrasons en cristallisoir discontinu et continu, Doctorat de l'Institut National Polytechnique de Toulouse, 20 Novembre **2003**.

[10] M. Hassoun, A. Vilela, F. Espitalier, O. Louisnard, R. David, Influence of ultrasound on cooling crystallisation in viscous medium, 4th International Conference for Conveying and Handling of Particulate Solids, Budapest 27–30 May **2003**, Hungary, p. 3.14–3.19

[11] D. Kaschiev, Nucleation, Basic theory with applications. Butterworth-Heinemann, Oxford, **2002**.

[12] O. Louisnard, F. Gomez, R. Grossier, Segregation of a liquid mixture by a radially oscillating bubble. Accepted in *J. Fluid Mech.* **2006**.

[13] N. Lyczko, F. Espitalier, O., Louisnard, J. Schwartzentruber, Effect of ultrasound on the induction time and the metastable zone widths of potassium sulphate, *Chemical Engineering Journal* **2002**, *86*, p. 233–241.

[14] A. Mersmann, Crystallisation technology handbook, 2nd edition, M. Dekker, Inc, New York, **2001**.

[15] J. W. Mullin, C. L. Leci, Evidence of molecular cluster formation in supersaturated solutions of citric acid, *Phil. Mag.* **1969**, *19*, 1075–1077.

[16] G. Ruecroft, D. Hipkiss, T. Ly, N. Maxted, P. W. Caims, Sonocrystallization: the use of ultraound for improved industrial crystallization, *Organic Process Research & Development*, **2005**, *9*, 923–932, 12–14.

[17] C. Virone, H. J. M. Kramer, G. M. Van Rosmalen, A. H. Stoop, T. W. Bakker, Ultrasound for reproducible nucleation in batch crystallization, 16th International Symposium on industrial crystallization, ISIC16, 11–14 September 2005, B13, volume *41*, p. 1195–1200, ISBN 3-18-091901-9, Ed. VDI Verlag GmbH, Düsseldorf, Germany **2005**.